Quasi-Fermi-Based Charge Transport Scheme for Device Simulation in Cryogenic, Wide Bandgap, and High-Voltage Applications

Zlatan Stanojević, *Senior Member, IEEE*, José María González-Medina, *Member, IEEE*, Franz Schanovsky, *Member, IEEE*, and Markus Karner, *Member, IEEE*

***Abstract*— We present a novel approach to solving the transport problem in semiconductors. We reformulate the drift-diffusion (DD) equations in terms of the quasi-Fermi-energies as solution variables; a drastic increase in numerical stability is achieved, which permits the simulation of devices at cryogenic temperatures as well as wide bandgap devices using double precision arithmetic, instead of extended precision arithmetic which would otherwise be required to solve these applications using regular DD.**

***Index Terms*— Cryogenic electronics, device simulation, drift-diffusion (DD), GaN, SiC, technology computer aided design (TCAD), wide bandgap semiconductors.**

I. Introduction

QUANTUM periphery devices, i.e., *classical* devices in circuits necessary to interface a qubit chip, and power-efficient wide bandgap devices have two things in common: their design is of high importance in their respective fields and they are notoriously difficult to simulate in technology computer aided design (TCAD).

Due to their vicinity to qubits on a Si-spin-based quantum chip [1], quantum periphery devices need to operate classically at very low temperatures, with the boiling point of helium at 4.2 K being commonly used as reference. The difficulties of TCAD device simulations under these conditions are rarely discussed in the literature but Dhillon et al. [2] provide valuable insight into a typical setup for a commercial device simulator. When presenting simulations of a 10 μm MOSFET at 5 K, the authors report that they used "transient simulation with extrapolation and Backward-Euler" to simulate transfer characteristics, which otherwise would have convergence difficulties in steady-state. They add, that they used 80-bit extended precision and that they set "the minimum carrier density [...] to 10^{-2000} cm^{-3} in the Newtonian iteration" (cf., discussion in Section IV-B).

Manuscript received 16 September 2022; revised 11 November 2022 and 7 December 2022; accepted 19 December 2022. Date of publication 30 December 2022; date of current version 24 January 2023. The review of this article was arranged by Editor S.-M. Hong. *(Corresponding author: Zlatan Stanojević.)*

The authors are with Global TCAD Solutions GmbH, 1010 Vienna, Austria (e-mail: z.stanojevic@globaltcad.com).

Color versions of one or more figures in this article are available at https://doi.org/10.1109/TED.2022.3232321.

Digital Object Identifier 10.1109/TED.2022.3232321

For wide bandgap materials, TCAD vendors regularly recommend using higher-than-double precision in their application examples, especially when facing low currents. Often seen as a technicality, this is again rarely discussed in the literature, however, Lophitis et al. [3] state: "Due to the very low intrinsic carrier concentration of WBG semiconductors, the expected leakage current is very low ($\approx 10^{-20}$ Acm^{-2}), which causes converge issues. To alleviate this, the numerical precision should be significantly high. This is achieved with the inclusion of certain keywords in the 'device (and circuit) simulation' tool command file (e.g., 'extended-precision' for SDevice tool of the Synopsys Sentaurus TCAD). Simulations that use extended arithmetic precision are computationally more intensive, therefore, the arithmetic precision should be increased in a trade-off manner up to a level that is able to provide a solution."

In this work, we aim to shed light on the particular issues plaguing these types of simulations and propose a solution that provides a robust and stable platform for simulations of devices at cryogenic temperatures and wide bandgap devices. Both of these applications feature a rich set of physical phenomena that each require careful modeling in TCAD. This article is not about that; we shall focus solely on the numerical issues found at the core of the transport scheme in device TCAD and how to solve them.

II. Numerical Cancellation in the DD Equation

It has been demonstrated in [4] that the drift-diffusion (DD) equation

$$\frac{\boldsymbol{J}_n}{\mu} = -n\nabla V - k_{\mathrm{B}}T\nabla n \tag{1}$$

(V is the effective band edge) suffers from what the authors describe as "catastrophic cancellation." Such cancellation appears whenever extremely small currents need to be represented in devices. This commonly occurs in reverse-biased diodes, or transistors in OFF-state. The phenomenon is exaggerated by cryogenic temperatures and wide band gaps since they tend to make tiny currents orders of magnitude smaller due to the reduced intrinsic carrier concentration of the semiconductor.

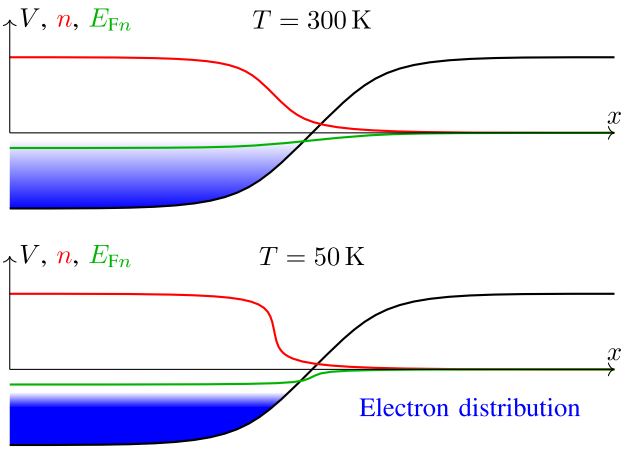

Fig. 1. Schematic of a p/n-junction in slight reverse bias; both potential and carrier gradients are substantial, yet the net current is tiny because drift and diffusion almost perfectly compensate. The tiny mismatch between drift and diffusion is what creates the net current.

Fig. 1 illustrates the circumstances in which catastrophic cancellation occurs. The (slightly) reverse-biased junction has a small leakage current flowing over it, however, inside the space charge region both the drift term $-n\nabla V$ and the diffusion term $-k_{\mathrm{B}}T\nabla n$ are rather large. In fact, they are almost the same in magnitude but have opposite signs. The resulting sum is the small but nonzero current.

The IEEE 754 double precision format has an epsilon of $2^{-53} \approx 10^{-16}$, which is the relative difference between two adjacent numbers represented in the format. If the drift and diffusion terms differ by less than that in the simulator, they will become the same number and their difference will be zero. However, zero current contradicts the physical reality that the current is nonzero. This causes the discretization to fail by producing a (near)-singular matrix and right-hand side.

This issue arises when the net current is 10^{16} times smaller in magnitude than the contributing drift and diffusion terms. While rare for silicon at room temperatures, this can readily occur at cryogenic temperatures and in wide bandgap semiconductors. The Scharfetter–Gummel (SG) discretization scheme [5], the Newton-Raphson iteration, and subnormal numbers in IEEE 754 complicate the picture somewhat but the basic realization remains. As long as the solution variable of the transport equation is the carrier concentration, the cancellation can occur.

In practice, i.e., in commercial and some non-commercial device simulators, this problem is addressed in software and hardware. Solvers are either statically compiled or can dynamically switch to use higher-precision floating-point formats, such as the 80-bit extended precision of the x86 architecture [2] or the 128-bit IEEE 754 quadruple precision format. This approach has several severe drawbacks.

1) Closed source solver libraries, such as parallel direct sparse solver (PARDISO), do not support number formats other than single and double precision [6]. Open source solver libraries, such as SuperLU, do not support higher precision formats either [7], but could *in principle* be refactored and recompiled to use extended or quadruple precision. Iterative solvers such as BiCGStab are simple enough to be easily refactored for higher precision but require preconditioners, which again are typically sourced from libraries.
2) The lack of readily available direct sparse solvers relegates the user to using iterative linear solvers for an already poorly conditioned problem.
3) Running the entire computation with higher precision incurs a significant runtime penalty. While not so severe for the 80-bit extended format, which has some hardware support in x86, quadruple precision's arithmetic is done in software resulting in huge slowdowns. The unavailability of high-performance solvers and preconditioners for the required precision exacerbates the slowdown, as does the generally slower convergence of cryogenic and wide bandgap device simulations.

III. Quasi-Fermi Transport (QFT)

We address the presented issue by reformulating (1). We change the equation variable from the carrier concentration to the quasi-Fermi energy $E_{\mathrm{F}n}$ quasi-Fermi level (QFL) or chemical potential η associated with the carrier type

$$\frac{\boldsymbol{J}_n}{\mu} = -n\nabla E_{\mathrm{F}n} \tag{2}$$

where the concentration itself is dependent on potential and quasi-Fermi energy

$$n = N_c\mathfrak{F}\left(\frac{E_{\mathrm{F}n} - V}{k_{\mathrm{B}}T}\right) \tag{3}$$

where $\mathfrak{F}$ can be an exponential for Maxwell–Boltzmann distribution, a Fermi-integral for Fermi-Dirac distribution, or a numerical energy quadrature combining a distribution function and a density-of-states function [8]. In any case, while (1) is linear for a fixed potential, (2) is nonlinear on its own. However, current in (2) is proportional to carrier concentration and driving force and no cancellation can occur. We shall call this mode Quasi-Fermi Transport or QFT.

The resulting law of current conservation

$$\nabla\cdot\boldsymbol{J}_n = -\nabla\cdot(\mu n\nabla\eta) = q_0\left(\frac{\partial n}{\partial t} + R\right) \tag{4}$$

is structurally similar to the Poisson equation, from which it inherits some useful properties.

1) In absence of recombination, the stationary equation's solutions is *monotonous* and is always bounded by the minimum and maximum of the contact Fermi energies.
2) The Laplace-like operator is positive semi-definite.

This general approach is not new and has been reported by multiple groups [4], [9], [10]. All these works use finite elements for discretization (FE/QFT), leveraging the similarity of (4) to the Poisson equation, for which finite element discretization is straightforward. However, the change of discretization results in deviations of the solution from the more established finite volume discretization, albeit small ones.

In this work, we present a finite-volume (FVM) discretization scheme for (2) which is fully consistent with FVM/SG/DD results of (1), while suffering none of its issues.

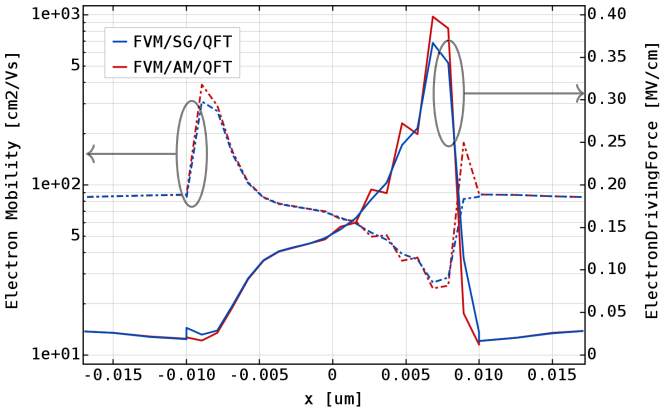

Fig. 2. Mobility and driving force inside a MOSFET channel in saturation, FVM/AM/QFT versus FVM/SG/QFT; the Caughey-Thomas-type velocity saturation model couples mobility to the driving force, while driving force depends on mobility through (2); the discretization error of the AM causes *wiggles* in both quantities, which are not present in FVM/SG/QFT or FVM/SG/DD.

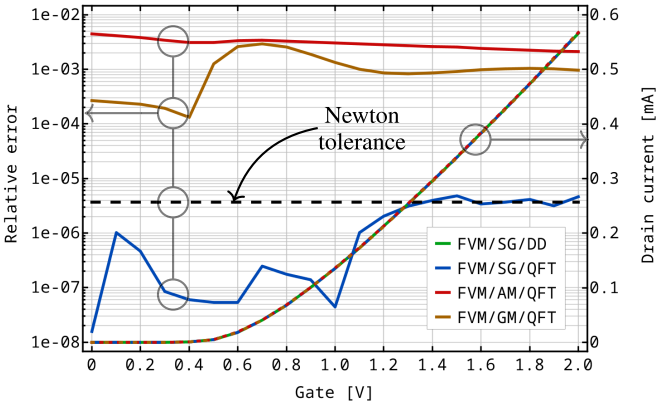

Fig. 3. Comparison of MOSFET transfer characteristics at $V_{DS} = 1$ V of FVM/SG/QFT, FVM/AM/QFT, and FVM/GM/QFT against FVM/SG/DD; both SG-discretized schemes produce identical results down to the Newton solver tolerance; FVM/AM/QFT and FVM/GM/QFT deviate substantially more but still less than 1%.

A. Finite-Volume QFT

In FVM, we assume that the potential V and the QFL are piecewise linear functions supported on the points of a mesh. Consequently, the carrier concentration shares that property. We need to approximate (2) along each edge $\{i, j\}$ of the mesh

$$\frac{J_{ij}}{\mu} = -n_{ij}\frac{\eta_j - \eta_i}{|\boldsymbol{r}_j - \boldsymbol{r}_i|} \tag{5}$$

requiring the carrier concentration n_{ij} at the center of the edge. The simplest approximations are the arithmetic mean (AM, $(n_i + n_j)/2$) giving FVM/AM/QFT, which is consistent with first-order finite elements, and the geometric mean (GM, $(n_i n_j)^{1/2}$) giving FVM/GM/QFT, which implies a piecewise linear QFL between the points i and j (for Boltzmann statistics). Both choices are numerically stable, unlike (1) when it is discretized in the same fashion as FVM/AM/QFT, i.e., by taking $(n_i + n_j)/2$ at the center of the edge. Neither FVM/AM/QFT nor FVM/GM/QFT are however fully consistent with the FVM/SG/DD version of (1).

Moreover, when using the velocity-saturation model, which results in a field-dependent mobility μ, the driving force in FVM/AM/QFT, becomes ragged, as shown in Fig. 2, and the scheme shows degraded convergence compared to DD.

B. SG for QFT

We have reformulated the SG discretization for the QFL, resulting in the following expression for the edge current (FVM/SG/QFT):

$$\frac{J_{i,j}}{\mu} = \sqrt{n_i n_j}\,\frac{\Delta/2}{\sinh(\Delta/2)}\,\frac{2k_{\mathrm{B}}T\sinh(\Delta_F/2)}{|\boldsymbol{r}_j - \boldsymbol{r}_i|} \tag{6}$$

with

$$\Delta = \frac{V_i - V_j}{k_{\mathrm{B}}T}, \quad \Delta_F = \frac{\eta_i - \eta_j}{k_{\mathrm{B}}T}. \tag{7}$$

Since this is the same formula as SG for DD but with a change of variables, it will yield exactly the same results as FVM/SG/DD, down to the error tolerance of the Newton algorithm, as can be seen in Fig. 3.

C. Fermi-Dirac Statistics

Fermi-Dirac statistics are crucial to cryogenic simulation, not only for accuracy but out of necessity, since the Maxwell–Boltzmann distribution becomes unbounded for $T \to 0$ K [11]. As mentioned in Section III, one additional benefit of QFT is that non-Boltzmann statistics can be applied in the evaluation of n, which is not as straightforward for the original formulation of DD in (1). Combining this with SG, turns (5) into an implicit integral equation of the current J_{ij}

$$\int_{\xi_j}^{\xi_i}\left(\frac{J_{ij}|\boldsymbol{r}_j - \boldsymbol{r}_i|}{\mu k_{\mathrm{B}}T N_c \mathfrak{F}(\xi)} + \Delta\right)^{-1} \mathrm{d}\eta = 1, \quad \xi := \frac{V - \eta}{k_{\mathrm{B}}T} \tag{8}$$

which has been discussed in [12] along with practical approximations for its solution. One of these approximations takes the shape of the Boltzmann-statistics-based SG formula (6) prefixed with a correction factor called the *inverse activity coefficient* [13], [14], [15]

$$\beta = \sqrt{\frac{\mathfrak{F}(\xi_i)\mathfrak{F}(\xi_j)}{\exp(\xi_i)\exp(\xi_j)}}. \tag{9}$$

It has been shown in [12] and [15], that for a sufficiently fine grid, this approximates the solution of (8) very well. The choice of β is also quite convenient for us because it allows us to *upgrade* (6) to Fermi-Dirac statistics without changing it at all and simply using the Fermi-integral to calculate n_i, n_j.

IV. Discussion

The FVM/SG/QFT and FVM/AM/QFT schemes have been implemented in the commercial simulator Minimos-NT [16], part of GTS Framework, alongside the existing FVM/SG/DD implementation. The implementation takes advantage of automatic differentiation, so the choice of discretization and thus the change of solution variables is transparent to other models, such as Schockley-Read-Hall.

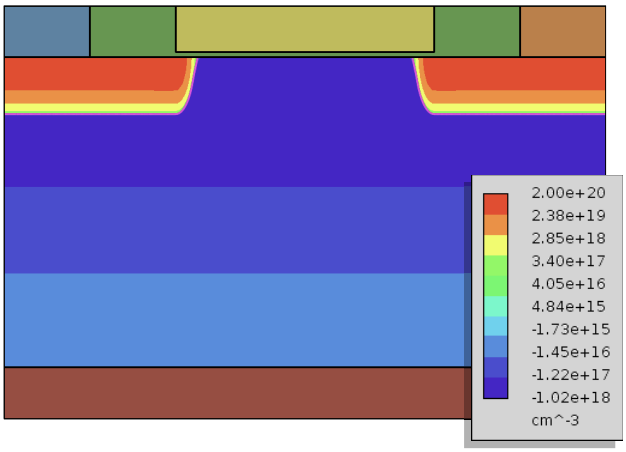

Fig. 4. Planar n-type MOSFET used in the benchmark; the printed gate length is 0.25 μm, gate oxide thickness is 5 nm, S/D doping is 10^{20} cm^{-3}, channel doping is 10^{19} cm^{-3}.

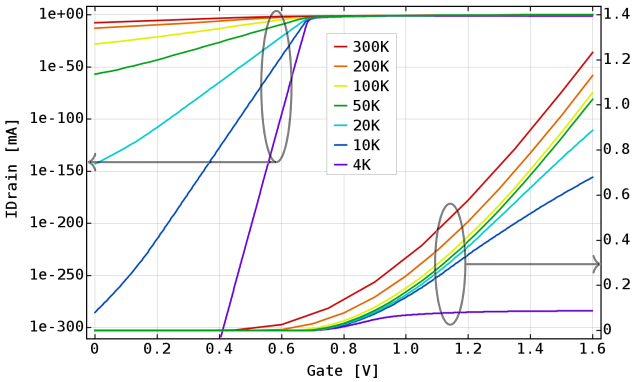

Fig. 5. MOSFET transfer characteristics from 300 K down to 4 K simulated using FVM/SG/QFT at $V_{DS} = 0.8$ V; despite only relying on double precision arithmetic, FVM/SG/QFT is capable of calculating contact currents down to 10^{310} A.

A. Simulation at Cryogenic Temperatures

To benchmark the FVM/SG/QFT at cryogenic temperatures, we use a $L = 0.25\,\mu$m, $W = 1\,\mu$m n-type bulk MOSFET, shown in Fig. 4. Transfer characteristics for the MOSFET are simulated with FVM/SG/DD and FVM/SG/QFT. The effects of cryogenic temperatures on device physics including mobility, velocity saturation, incomplete dopant ionization, quantum correction, and so on have been discussed at length elsewhere [17]. We will not cover these here but instead focus on transport only. Tail states [18] are purposefully omitted here in order to see how far the numerical stability of the scheme can be pushed. Our setup includes the Poisson equation and the QFT or DD equations for electrons and holes with the Minimos mobility model [19]. The mobility is hardly adequate for cryogenic temperatures but provides a non-constant, temperature, dopant, and field-dependent mobility for our benchmark.

Fig. 5 shows the transfer characteristics of the MOSFET, simulated with FVM/SG/QFT from 300 K down to 4 K. The characteristics were obtained using steady-state simulations. In contrast, no drain currents below 10^{-25} A could be obtained from FVM/SG/DD simulations.

To address the inherent instabilities at low-temperature [17], the following bias-ramping scheme was used for the transfer characteristics.

1) At $V_{DS} = 0$ V, the initial gate voltage V_G is applied, and the solution is obtained without QFT, but instead simply using (3) with $E_{Fn} = 0$ eV to obtain carrier concentrations self-consistently since the device is in equilibrium.
2) QFT is enabled and V_{DS} is ramped to its target value. The step size is chosen to be a multiple of $k_B T$.
3) V_G is stepped across the desired range. Here, the step size is also chosen to be a multiple of $k_B T$.

Note that all simulations were performed with IEEE 754 double precision arithmetic and used PARDISO [6] as the linear solver backend. At approximately 20 K, the carrier concentration underflows the double precision format, i.e., it becomes lower than the smallest positive number representable in double precision ($\approx 10^{-310}$) and thus is represented by an exact zero. This will zero-out (2) and (5) resulting in a singular matrix. We apply a row-rescaling to shift the equation back into the appropriate range for double precision. The same issue also arises for the contact current, which drops below 10^{-310} A near 10 K. This however, cannot be remedied as Minimos-NT uses double precision for all its I/O routines and file formats. It is however remarkable, that the simulations still converge in this regime, even though the contact current cannot be evaluated.

The mesh density in the device is critical at these low temperatures. This can be understood from the Fermi-Dirac distribution, which becomes more and more step-like at low temperatures. Consequently, the QFL inside the device becomes more and more step-like too, necessitating finer mesh resolutions to ensure convergence at the lowest temperatures.

B. Wide bandgap Devices

High-voltage devices are an application where the SG-extension of QFT to FVM/SG/QFT is essential. At high fields and driving forces, SG continuously transfers weight to the coefficient belonging to the "upstream" end of an edge $\{i, j\}$, thus smoothly transitions between central and one-sided differencing. This is equally true for FVM/SG/DD and FVM/SG/QFT in (5). The FVM/AM/QFT approach weights both sides equally resulting in central differencing under all conditions. Thus FVM/AM/QFT exhibits less stable convergence for high-voltage applications.

We use a simple planar p/n-diode shown in Fig. 6 (top) to benchmark the high-voltage capabilities of FVM/SG/QFT. We first simulate the diode with Si as the semiconductor material to establish a baseline comparison between FVM/SG/QFT and FVM/SG/DD. The diode characteristics shown in Fig. 7 coincide for both methods, which is to be expected. However, the FVM/SG/DD electron current density at reverse bias in Fig. 6 (bottom) exhibits spurious behavior near the cathode, which can be observed in detail in Fig. 8 and is a telltale sign of the cancellation effect discussed in Section II. A similar

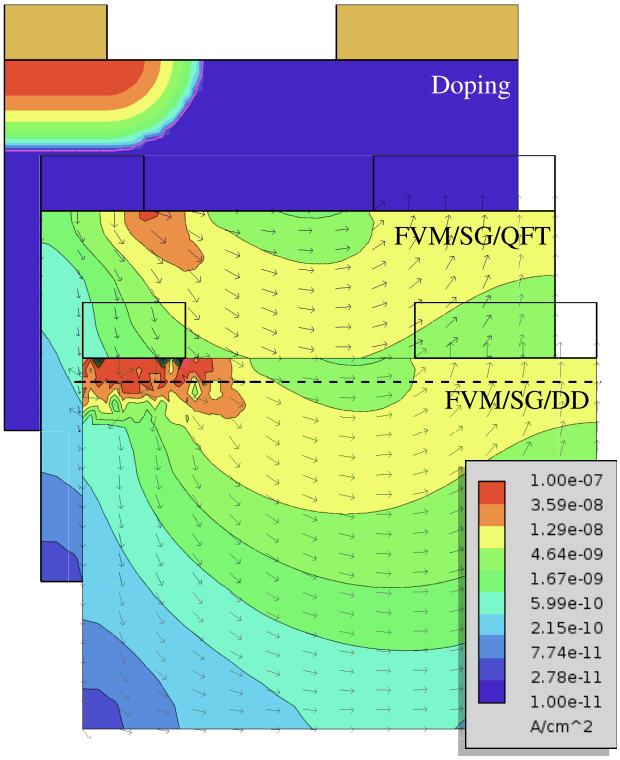

Fig. 6. Top: diode structure; cathode doping is 10^{20} cm^{-3}, cathode width is 90 nm; middle: electron current density at $V = -5$ V simulated with FVM/SG/QFT; bottom: same with FVM/SG/DD; the dashed line indicates cut position for Fig. 8.

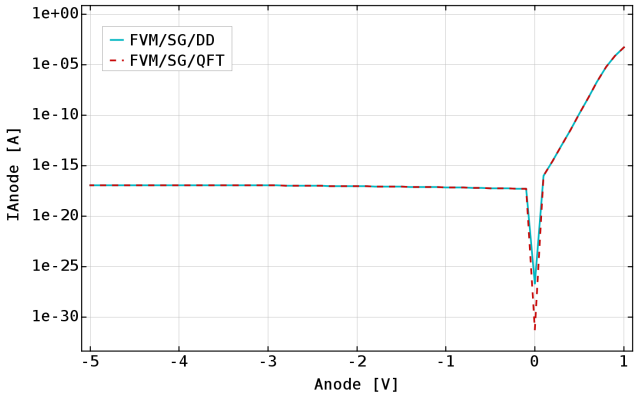

Fig. 7. Characteristic of the Si-diode simulated with FVM/SG/QFT and FVM/SG/DD; there is no appreciable difference between the two results.

discrepancy of internal and contact current stability was also reported in [4].

To test the limits of both FVM/SG/QFT and FVM/SG/DD, we replace the semiconductor material of the diode with SiC, and increase the voltage range to span from -50 to 5 V. As was the case for the MOSFET, we have purposefully omitted generation models such as impact ionization in order to get an extremely low reverse-bias current for this test.

Fig. 9 clearly shows the breakdown of the FVM/SG/DD scheme, which is unable to reproduce currents below 1 V forward bias. It's important to remark here that both simulations converged on all bias points. Minimos-NT and

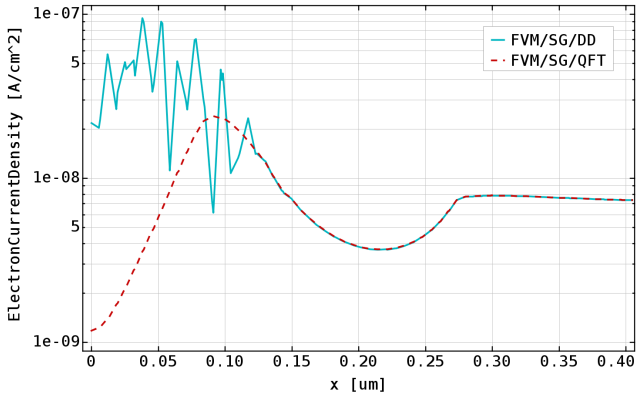

Fig. 8. Electron current density from FVM/SG/QFT and FVM/SG/DD at $V = -5$ V along the cut indicated in Fig. 6.

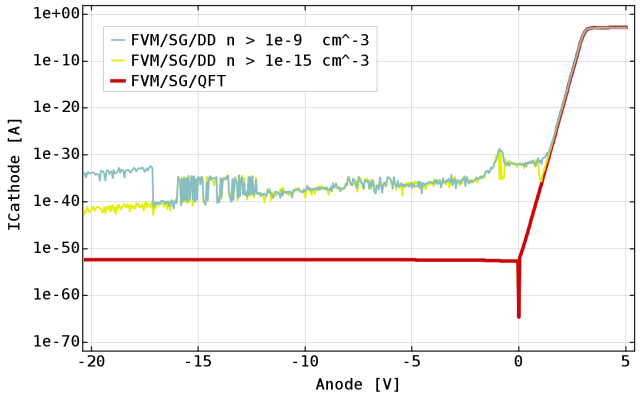

Fig. 9. Characteristic of the SiC-diode simulated with FVM/SG/QFT and FVM/SG/DD; DD is entirely incapable of simulating the device in reverse bias. Reducing the minimum carrier concentration in DD by 10^{-6} does not yield any improvements, hinting that the issue is fundamental to the DD scheme itself.

other commercial simulators [2] employ a lower carrier concentration bound, such that the concentration, should it drop below that value, is automatically corrected. The correction is done after each Netwon iteration and prevents carrier concentrations from becoming zero or negative, which would immediately cause the following iteration to fail during assembly. We reduced this bound from its default value of 10^{-9} to -10^{-15} cm^{-3} to ensure that it is not that which is limiting the simulations with FVM/SG/DD scheme. As can be seen in Fig. 9, this is not the case. It is noteworthy, that QFT does not require such bounds, as the carrier concentration is positive by construction – save for the discussed case where it drops below 10^{-310} cm^{-3}.

V. Conclusion

We have presented an FVM quasi-Fermi-energy-based formulation of the DD model with an adapted SG discretization scheme (FVM/SG/QFT) that is fully consistent with the FVM/SG/DD formulation from the literature. The implementation of the FVM/SG/QFT approach exhibits vastly superior numerical stability and accuracy, allowing steady-state simulation of devices at temperatures as low as 4 K as well as of wide bandgap devices at high voltages.

REFERENCES

[1] M. Vinet et al., "Towards scalable silicon quantum computing," in *IEDM Tech. Dig.*, Dec. 2018, pp. 6.5.1–6.5.4, doi: 10.1109/IEDM.2018.8614675.

[2] P. Dhillon, N. C. Dao, P. H. W. Leong, and H. Y. Wong, "TCAD modeling of cryogenic nMOSFET ON-state current and subthreshold slope," in *Proc. Int. Conf. Simulation Semiconductor Processes Devices (SISPAD)*, Sep. 2021, pp. 255–258, doi: 10.1109/SISPAD54002.2021.9592586.

[3] N. Lophitis, A. Arvanitopoulos, S. Perkins, and M. Antoniou, "TCAD device modelling and simulation of wide bandgap power semiconductors," in *Disruptive Wide Bandgap Semiconductors, Related Technologies, and Their Applications*. Rijeka, Croatia: InTech, Sep. 2018. [Online]. Available: https://www.intechopen.com/chapters/60792

[4] E. C. Dumitrescu, M. M. Wilkins, and J. J. Krich, "Simudo: A device model for intermediate band materials," *J. Comput. Electron.*, vol. 19, no. 1, pp. 111–127, Nov. 2019, doi: 10.1007/s10825-019-01414-3.

[5] D. L. Scharfetter and H. K. Gummel, "Large-signal analysis of a silicon Read diode oscillator," *IEEE Trans. Electron Devices*, vol. ED-16, no. 1, pp. 64–77, Jan. 1969, doi: 10.1109/T-ED.1969.16566.

[6] *OneMKL PARDISO—Parallel Direct Sparse Solver Interface*. Accessed: Dec. 28, 2022. [Online]. Available: https://www.intel.com/content/www/us/en/develop/documentation/onemkl-developer-reference-c/top/sparse-solver-routines/onemkl-pardiso-parallel-direct-sparse-solver-iface.html

[7] X. S. Li, J. W. Demmel, J. R. Gilbert, iL. Grigori, M. Shao, and I. Yamazaki, "SuperLU users' guide," Lawrence Berkeley Nat. Lab., Berkeley, CA, USA, Tech. Rep. LBNL-44289, Sep. 1999. [Online]. Available: https://portal.nersc.gov/project/sparse/superlu/ug.pdf

[8] A. Toral-Lopez, H. Santos, E. G. Marin, F. G. Ruiz, J. J. Palacios, and A. Godoy, "Multi-scale modeling of 2D GaSe FETs with strained channels," *Nanotechnology*, vol. 33, no. 10, Dec. 2021, Art. no. 105201, doi: 10.1088/1361-6528/ac3ce2.

[9] D. J. Cummings, M. E. Law, S. Cea, and T. Linton, "Comparison of discretization methods for device simulation," in *Proc. Int. Conf. Simulation Semiconductor Processes Devices*, Sep. 2009, pp. 1–4, doi: 10.1109/SISPAD.2009.5290236.

[10] T. Weingartner, M. E. Law, K. Green, A. Thomas, H. Johnson, and P. Leger, "TCAD comprehensive silicon strain model using finite element quasi-Fermi discretization," in *Proc. Int. Conf. Simulation Semiconductor Processes Devices (SISPAD)*, Sep. 2021, pp. 242–246, doi: 10.1109/SISPAD54002.2021.9592582.

[11] M. Kantner and T. Koprucki, "Numerical simulation of carrier transport in semiconductor devices at cryogenic temperatures," *Opt. Quantum Electron.*, vol. 48, no. 12, pp. 1–7, Nov. 2016, doi: 10.1007/s11082-016-0817-2.

[12] P. Farrell, T. Koprucki, and J. Fuhrmann, "Computational and analytical comparison of flux discretizations for the semiconductor device equations beyond Boltzmann statistics," *J. Comput. Phys.*, vol. 346, pp. 497–513, Oct. 2017, doi: 10.1016/j.jcp.2017.06.023.

[13] M. Bessemoulin-Chatard, "A finite volume scheme for convection–diffusion equations with nonlinear diffusion derived from the Scharfetter–Gummel scheme," *Numerische Math.*, vol. 121, no. 4, pp. 637–670, Feb. 2012, doi: 10.1007/s00211-012-0448-x.

[14] T. Koprucki and K. Gärtner, "Discretization scheme for drift-diffusion equations with strong diffusion enhancement," *Opt. Quantum Electron.*, vol. 45, no. 7, pp. 791–796, Mar. 2013, doi: 10.1007/s11082-013-9673-5.

[15] J. Fuhrmann, "Comparison and numerical treatment of generalised Nernst–Planck models," *Comput. Phys. Commun.*, vol. 196, pp. 166–178, Nov. 2015, doi: 10.1016/j.cpc.2015.06.004.

[16] Global TCAD Solutions. *Minimos-NT*. Accessed: Dec. 28, 2022. [Online]. Available: http://www.globaltcad.com/minimos-nt and http://www.globaltcad.com/en/products/gts-framework.html

[17] S. Jin, A.-T. Pham, W. Choi, M. A. Pourghaderi, U. Kwon, and D. S. Kim, "Considerations for DD simulation at cryogenic temperature," in *Proc. Int. Conf. Simulation Semiconductor Processes Devices (SISPAD)*, Sep. 2021, pp. 251–254, doi: 10.1109/SISPAD54002.2021.9592572.

[18] A. Beckers, F. Jazaeri, and C. Enz, "Theoretical limit of low temperature subthreshold swing in field-effect transistors," *IEEE Electron Device Lett.*, vol. 41, no. 2, pp. 276–279, Feb. 2020, doi: 10.1109/LED.2019.2963379.

[19] S. Selberherr, W. Hänsch, M. Seavey, and J. Slotboom, "The evolution of the MINIMOS mobility model," *Solid-State Electron.*, vol. 33, no. 11, pp. 1425–1436, Nov. 1990, doi: 10.1016/0038-1101(90)90117-w.